

RESEARCH OUTPUTS / RÉSULTATS DE RECHERCHE

Synthesis and evaluation of heterocycle structures as potential inhibitors of *Mycobacterium tuberculosis* UGM

Maaliki, Carine; Fu, Jian; Villaume, Sydney; Viljoen, Albertus; Raynaud, Clément; Hammoud, Sokaina; Thibonnet, Jérôme; Kremer, Laurent; Vincent, Stéphane P.; Thiery, Emilie

Published in:
Bioorganic and Medicinal Chemistry

DOI:
[10.1016/j.bmc.2020.115579](https://doi.org/10.1016/j.bmc.2020.115579)

Publication date:
2020

Document Version
Publisher's PDF, also known as Version of record

[Link to publication](#)

Citation for pulished version (HARVARD):
Maaliki, C, Fu, J, Villaume, S, Viljoen, A, Raynaud, C, Hammoud, S, Thibonnet, J, Kremer, L, Vincent, SP & Thiery, E 2020, 'Synthesis and evaluation of heterocycle structures as potential inhibitors of *Mycobacterium tuberculosis* UGM', *Bioorganic and Medicinal Chemistry*, vol. 28, no. 13, 115579.
<https://doi.org/10.1016/j.bmc.2020.115579>

General rights

Copyright and moral rights for the publications made accessible in the public portal are retained by the authors and/or other copyright owners and it is a condition of accessing publications that users recognise and abide by the legal requirements associated with these rights.

- Users may download and print one copy of any publication from the public portal for the purpose of private study or research.
- You may not further distribute the material or use it for any profit-making activity or commercial gain
- You may freely distribute the URL identifying the publication in the public portal ?

Take down policy

If you believe that this document breaches copyright please contact us providing details, and we will remove access to the work immediately and investigate your claim.



Synthesis and evaluation of heterocycle structures as potential inhibitors of *Mycobacterium tuberculosis* UGM

Carine Maaliki^a, Jian Fu^b, Sydney Villaume^b, Albertus Viljoen^c, Clément Raynaud^c, Sokaina Hammoud^a, Jérôme Thibonnet^a, Laurent Kremer^{c,d}, Stéphane P. Vincent^b, Emilie Thiery^{a,*}

^a Laboratoire Synthèse et Isolement de Molécules Bioactives (SIMBA, EA 7502), Université de Tours, Faculté de Pharmacie, Parc de Grandmont, 31 Avenue Monge, 37200 Tours, France

^b Department of Chemistry, University of Namur, Rue de Bruxelles 61, 5000 Namur, Belgium

^c Institut de Recherche en Infectiologie de Montpellier (IRIM), CNRS UMR 9004, Université de Montpellier, 34293 Montpellier, France

^d INSERM, IRIM, 34293 Montpellier, France

ARTICLE INFO

Keywords:

Heterocycles
Mycobacterium tuberculosis
UDP-galactopyranose mutase
Inhibitor
Docking

ABSTRACT

In this study, we screen three heterocyclic structures as potential inhibitors of UDP-galactopyranose mutase (UGM), an enzyme involved in the biosynthesis of the cell wall of *Mycobacterium tuberculosis*. In order to understand the binding mode, docking simulations are performed on the best inhibitors. Their activity on *Mycobacterium tuberculosis* is also evaluated. This study made it possible to highlight an “oxazepino-indole” structure as a new inhibitor of UGM and of *M. tuberculosis* growth *in vitro*.

1. Introduction

Tuberculosis (TB) is the world's deadliest infectious disease, responsible for 1.8 million deaths every year. According to the WHO report “Antibacterial agents in clinical development” published in 2017, inadequate new treatment options exist for antibiotic-resistant TB.¹ The emergence of drug-resistant strains of *Mycobacterium tuberculosis* (*Mt*) decreases the efficacy of treatment, which requires a combination of at least three antibiotics as first-line therapy. In the case of multi- and extensively-drug-resistant (MDR-TB and XDR-TB) strains, complex, prolonged, costly and highly toxic multidrug second-line therapy is required and only 30–50% of patients are treated successfully. In more than 70 years, only two antibiotics for the treatment of drug-resistant TB reached the market, and seven are currently being evaluated in clinical trials.¹ The development of new strategies and new molecular scaffolds is, therefore, necessary to counter the increasing threat of antimicrobial resistance and to propose new therapeutic options for TB treatment.²

Mt has a complex lifestyle involving several developmental stages. Its success results from its remarkable capacity to survive within the infected host, where it can persist in a non-replicating state for several decades in granulomas. The survival strategies developed by *Mt* are essentially linked to the presence of an unusual cell wall, which consists

of two major layers (Fig. 1). The highly impermeable outer layer is composed of mycolic acids consisting of 70–90 carbon-containing fatty acids. The inner layer consists of peptidoglycan. These two layers are covalently tethered via the connecting polysaccharide arabinogalactan (AG).³ AG itself comprises three regions: i) a disaccharide ‘linker’ attached to the peptidoglycan, ii) the galactofuran [(→6)-β-D-Galf-(1 → 5)-β-D-(Gal)]_n which is attached to the linker unit, and iii) a complex arabinan linked to the galactofuran and representing the site of attachment of mycolic acids. These are oriented perpendicular to the plane of the membrane, providing a barrier responsible for the natural resistance of *Mt* to many antibiotic classes, and contribute to the physiopathological aspects characterizing TB. In addition, within this lipid environment are intercalated several glycolipids with exotic structures, such as the phthiocerol dimycocerosate, phenolic glycolipids, trehalose dimycolate (TDM) or sulfolipids. The role of these lipids in signaling events, pathogenesis, immune response and even in coughing has been established.⁴

Therefore, the integrity of both the mycolic acid-arabinogalactan-peptidoglycan skeleton (mAGP) and the outer mycomembrane leaflet of extractable lipids hinges on the integrity of the arabinan moiety of AG. In addition to its crucial structural role, arabinan exhibits also specific immunomodulatory activities although these functions have mostly been connected to the arabinan part of lipoarabinomannan that shares

* Corresponding author.

E-mail address: emilie.thiery@univ-tours.fr (E. Thiery).

<https://doi.org/10.1016/j.bmc.2020.115579>

Received 27 March 2020; Received in revised form 26 May 2020; Accepted 29 May 2020

Available online 02 June 2020

0968-0896/ © 2020 Elsevier Ltd. All rights reserved.

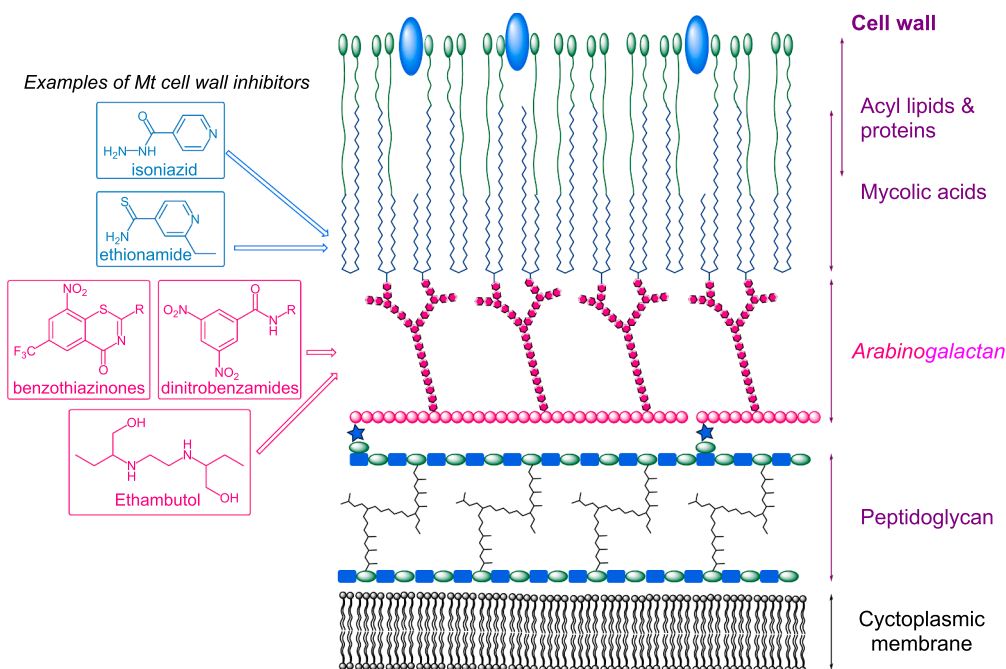


Fig. 1. Schematic structure of the *M. tuberculosis* cell envelope. Structures and sites of action of several anti-TB drugs targeting the cell wall are shown. Chemical entities inhibiting AG biosynthesis are in pink.

structural features with mAGP.⁵

During the past two decades, intensive efforts conducted to the discovery of new leads for TB drug development using either target-based or cell-based approaches and the molecular mechanisms of action of several anti-TB drugs were deciphered.⁶ Several major anti-TB agents disrupt the biosynthesis of cell wall components. For instance, isoniazid and ethionamide are key inhibitors of mycolic acid biosynthesis, while ethambutol and the recently identified chemical classes the benzothiazinones and dinitrobenzamide derivatives inhibit biosynthesis of arabinan (Fig. 1).⁷

Several enzymes are involved in the biosynthesis of the galactan moiety of the cell wall but marketed antitubercular agents targeting this polysaccharide are currently lacking. One such enzyme is the UDP-galactopyranose (UDP-Galp) mutase (UGM), which catalyzes the interconversion of UDP-galactopyranose (UDP-Galp) into UDP-galactofuranose (UDP-Galf) (Scheme 1), subsequently used by the Galf transferases GlfT1 and GlfT2 to polymerize the galactofuran subunit of arabinogalactan.⁸ Interestingly, UGM, which is absent in humans, is essential for the growth of mycobacteria, therefore representing a privileged and validated therapeutic target.⁹

Until recently, the search for UGM inhibitors has mainly focused on the preparation of substrate analogues.¹⁰ However, screening studies have also shown that heterocyclic molecules can exhibit strong interactions with the catalytic site of the enzyme.¹¹ Recently, various heterocyclic compounds, including flavonoids,¹² acylhydrazones¹³ and thiazol-2-amines¹⁴ were shown to inhibit *Mt* UGM.

Herein, we present the screening of novel heterocyclic compounds for *Mt* UGM inhibition. We explored the relative levels of UGM inhibition by the three scaffolds represented in Fig. 2. Indeed, butenolides and indole derivatives are important pharmacophores that have not been explored for UGM inhibition yet. To evaluate the binding mode of

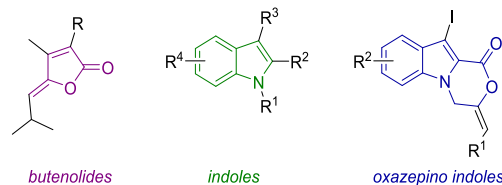


Fig. 2. Three heterocyclic structures studied for *Mt* UGM inhibition.

the best inhibitors, molecular docking experiments are described. The *in vitro* anti-bacterial activities of the best UGM inhibitors are also reported.

2. Results and discussion

2.1. Initial screening

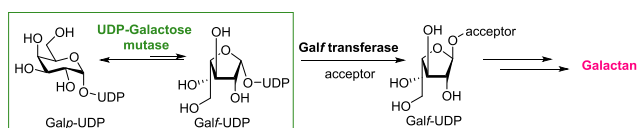
Two distinct biochemical assays have been developed to evaluate the binding affinity of small molecules towards purified *Mt* UGM. An HPLC-based assay allows the monitoring of the conversion of the substrate, UDP-Galf, into UDP-Galp using *Mt* UGM in its active reduced form. Percentages of inhibition are usually described with this assay. The concentration of UDP-Galf (25 μ M) was chosen to be close to its K_m (23 μ M for *Mt*UGM).¹⁰

A higher-throughput fluorescence polarization (FP) assay has also been developed and exploited on the non-reduced form of the enzyme.¹⁵ The latter is based on the competition between the screened ligand(s) and a fluorescent probe and can be performed in multi-well plates.

Our methodology consisted first to screen chemical libraries by FP at inhibitor concentrations of 100 μ M and 1 mM (only the values at 1 mM are displayed in Tables 1–3). When the percentage of inhibition was greater than 30% at 1 mM, the affinity of the inhibitors (K_d 's) was determined using the FP assay.¹⁶

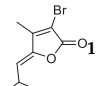
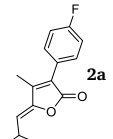
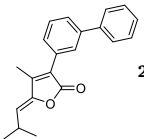
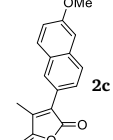
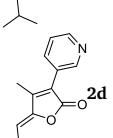
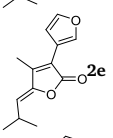
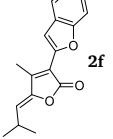
Being much more demanding, the HPLC assay was only used for the very best hits.

Butenolides and their derivatives represent a large family of natural products. Since the 1970's, many furan heterocycles have been isolated



Scheme 1. Isomerization of UDP-Galp by UGM and elaboration of galactan.

Table 1
The *Mt* UGM inhibition data for the butenolide series.

Entry	Compound	<i>Mt</i> UGM Inhibition ^[a] [%]
1		7.3
2		9.0
3		19.2
4		7.4
5		3.0
6		5.2
7		0

^a FP inhibition assay conditions: [inhibitor] = 1 mM, non-reduced enzyme, [*Mt* UGM] = 580 nM, [fluorescent probe] = 18 nM.

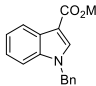
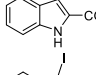
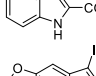
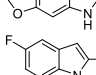
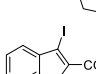
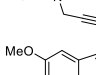
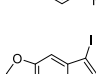
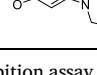
with a wide range of biological activities. As examples, xerulin and derivatives are inhibitors of cholesterol biosynthesis¹⁷ while trenolin¹⁸ and freelyngine¹⁹ display antibiotic activities.

To generate a first representative set of butenolides **2a-f**, we developed a new stereoselective synthetic strategy of (*E*)- α -substituted β -methyl (*Z*)- γ -alkylidene butenolides (Scheme 2). As previously reported for β -iodopropenoic acid derivatives,²⁰ the first step is based on the cross-coupling-heterocyclization reaction sequence between terminal alkynes and (*E*)-2,3-dibromobutenoic acid in order to obtain α -bromo β -methyl (*Z*)- γ -isobutylidene furan-2-one **1** (Scheme 2). The presence of the bromide in the α position allows the modification of the furanone moiety via Suzuki coupling, providing access to a wide panel of α -substituted furan-2-one **2** (Scheme 2, Table 1).

The inhibition data for compounds **1** and **2a-f** are reported in Table 1. All butenolides were tested at 1 mM using the FP-based assay. However, none of them displayed a satisfactory inhibition level, encouraging us to explore two other targeted scaffolds.

We next examined the indole series of molecules. These heterocycles are present in many bioactive molecules, including antituberculous agents.²¹ According to procedures previously described in the literature,²² ethyl 3-iodo-1*H*-indole-2-carboxylates **5** were prepared from commercially available compounds **4** in the presence of *N*-iodosuccinimide (Scheme 3). The propargylation of compounds **4** and **5** led to

Table 2
The *Mt* UGM inhibition data for the indole series.

Entry	Compound	Inhibition <i>Mt</i> UGM [%] ^[a]	K_d ^[b] [μ M] <i>Mt</i> UGM
1		5.1	–
2		2.0	–
3		11.5	–
4		23.1	–
5		0	–
6		7.4	–
7		15.0	–
8		46.2	220 \pm 2

^a FP inhibition assay conditions: [inhibitor] = 1 mM, non-reduced enzyme, [*Mt* UGM] = 580 nM, [fluorescent probe] = 18 nM. ^b FP assay conditions: [inhibitors] = 0–1 mM, non-reduced enzyme, [*Mt* UGM] = 580 nM, [fluorescent probe] = 18 nM.

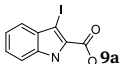
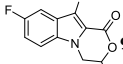
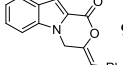
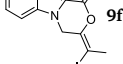
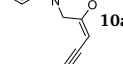
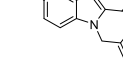
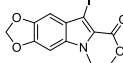
compounds **6** and **7**, respectively. Saponification of carboxylated indoles **7** yielded the corresponding acids **8**. Molecules **4a-d**, **6**, **7** and **8a-d** were selected for preliminary UGM inhibition assays because if a hit is discovered, they offer the possibility to be further derivatized for a structure activity relationship (SAR) study.

The UGM inhibitory activity of a selection of eight indoles was evaluated (Table 2). The tested compounds were very poor inhibitors (Entries 1–7), except product **8d** (Entry 8) which reduced the activity of *Mt* UGM to 46% (entry 8). However, **8d** showed low affinity for *Mt* UGM (K_d = 220 μ M). As compared to the other molecules in this series, the presence of both the dioxolane ring and the free carboxylic acid on the indole scaffold appears important for UGM inhibition (Entries 3–4 and 6–8).

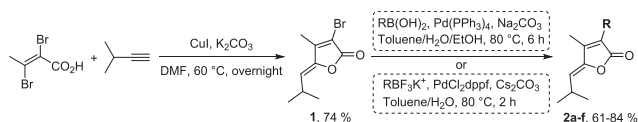
Finally, we prepared a series of tricyclic indoles based on synthetic protocols described in the literature (Scheme 4).²² The iodocyclisation of indoles **8** in the presence of silver nitrate, diiodine and sodium carbonate in tetrahydrofuran led to the oxazinoindole compounds **9**. The functionalization of vinyl iodine by Sonogashira coupling made it possible to generate products **10**.

The inhibition data for compounds **9** and **10** are reported in Table 3. Compound **9a** displayed a poor inhibitory activity for *Mt* UGM (FP assay) for the enzyme (Entry 1). The functionalization of the indole cycle by a fluorine lead to a decrease in activity (Entry 2). The same effect is observed when a methyl or a phenyl is present on the vinylic pattern (Entries 3 and 4). In contrast, compounds **10** showed good inhibitory activities and affinities for *Mt* UGM (Entries 5–7). K_d values for molecules **10a**, **10c** and **10d** were found in the same range (58–66 μ M). To make sure that these molecules are not false positive, we evaluated them by the HPLC assay. More significant inhibitory differences could be measured: molecule **10c** displayed a 95% inhibition level as compared to 73% for **10a** and 60% for **10d**. Such differences between these assays are not surprising as the FP assay is conducted with the non-reduced enzyme against a fluorescent probe whereas the HPLC uses the

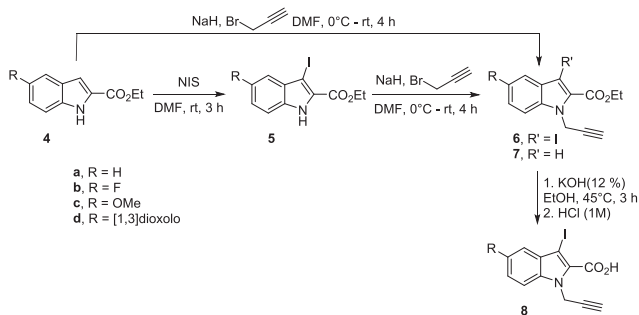
Table 3
The *Mt* UGM inhibition data for the “oxazino-indole” series.

Entry	Compound	Inhibition <i>Mt</i> UGM [%]	$K_d^{[b]}$ [μ M]	<i>Mt</i> UGM
1		61.6 ^[a]	2000	
2		19.1 ^[a]	–	
3		22.8 ^[a]	–	
4		14.9 ^[a]	–	
5		72.9 \pm 3.3 ^[c]	66 \pm 1.5	
6		95.5 \pm 0.5 ^[c]	61.3 \pm 1.4	
7		60.2 \pm 3.6 ^[c]	58.3 \pm 1.2	

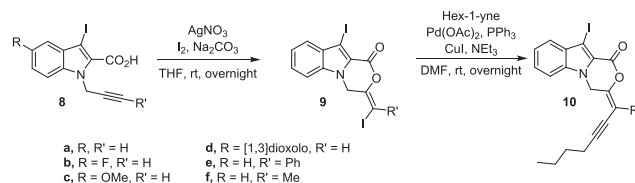
^aInhibition assay conditions: [inhibitor] = 1 mM, non-reduced enzyme, [*Mt* UGM] = 580 nM, [fluorescent probe] = 18 nM. ^b FP assay conditions: [inhibitors] = 0–1 mM, non-reduced enzyme, [*Mt* UGM] = 580 nM, [fluorescent probe] = 18 nM. ^c HPLC inhibition assay conditions: [inhibitor] = 0.5 mM, [*Mt* UGM] = 25 nM, [UDP-Galf] = 25 μ M.



Scheme 2. Synthesis of α -substituted β -methyl γ -alkylidene butenolides.



Scheme 3. Synthesis of indole derivatives.



Scheme 4. Synthesis of tricyclic indole derivatives.

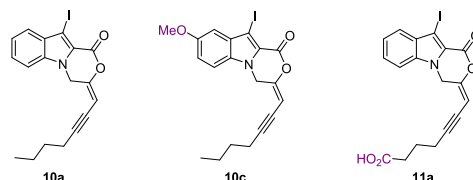


Fig. 3. Molecules subjected to docking simulations.

reduced UGM against the natural substrate UDP-Galf.

2.2. Docking of “oxazepino indole” compounds with *Mt* UGM

To evaluate their binding modes, the best inhibitory candidates (**10a** and **10c**, Fig. 3) were subjected to docking simulations. All modelling calculations were performed by using *Mt* UGM crystal structures in its closed conformation (PDB code: 4RPG).¹⁰ The UDP-galactose binding pocket of UGM consists of a galactose sub-pocket close to the FAD cofactor, a pyrophosphate sub-pocket where two arginine residues (Arg 292 and 180) can be found and a more hydrophobic uridine binding pocket.

For molecules **10a** and **10c**, only one binding mode could be observed: the tricyclic indole core strongly interacts with the residues of the uridine sub-pocket while the alkynyl chain lies within the pyrophosphate pocket without making noticeable contacts (Fig. 4 and Supplementary information). The methoxy group in **10c** does not significantly change the position of the molecule in the cavity as compared to **10a** and makes a contact with asparagine 284. In order to optimize interactions, the modelling was carried out with a tricyclic “oxazepino indole” bearing a carboxylic acid (molecule **11a**, Fig. 3). The binding mode remains the same as for **10a** and **10c** with characteristic contacts in the uridine pocket with residues Tyr366, Leu141, Thr162, Tyr161 and Tyr191. However, a clear interaction with Arg292 and the carboxylate could be observed. Such an attractive interaction could induce a better affinity for *Mt* UGM. We thus concentrated efforts on the synthesis of compound **11a**.

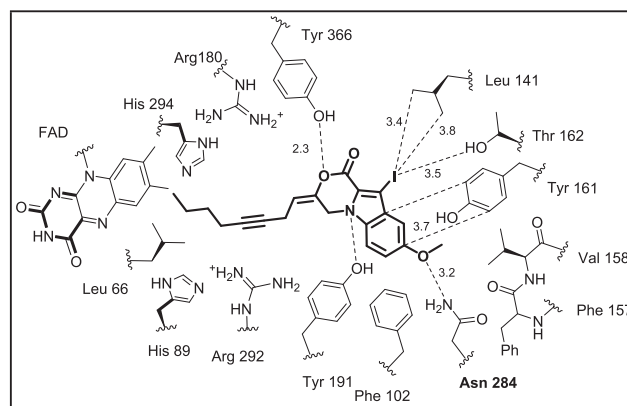
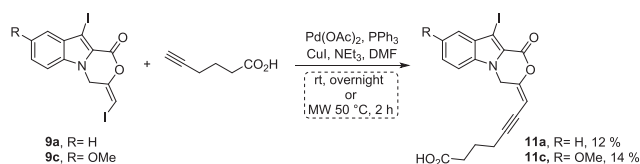


Fig. 4. Interaction map of **10c** with *Mt* UGM.



Scheme 5. Synthesis of compounds 11a and 11c.

Table 4

The *Mt* UGM inhibition data for the compounds 11a and 11c.

Entry	Compound	Inhibition ^[a] <i>Mt</i> UGM [%]	K _d ^[b] [μM] <i>Mt</i> UGM
1	11a, R = H	84.0	56.8 ± 1.2
2	11c, R = OMe	83.5	33.8 ± 1.2

^a [inhibitor] = 1 mM, non-reduced enzyme, [*Mt* UGM] = 580 nM, [fluorescent probe] = 18 nM. ^b FP assay conditions: [inhibitors] = 0–1 mM, non-reduced enzyme, [*Mt* UGM] = 580 nM, [fluorescence probe] = 18 nM.

2.3. Synthesis and evaluation of new “oxazepino-indole” compounds

The promising results obtained with molecules **10** prompted us to explore further this design by incorporating a polar carboxylic acid to improve the water solubility and find evidence of hydrophobic/hydrophilic effects in the association of **10** with UGM. Compounds **11a** and **11c** were respectively prepared under Sonogashira conditions from iodoalkenes **9a** and **9c** (Scheme 5). The reaction was performed at room temperature or at 50 °C under microwave irradiation. Compounds **11** were partially degraded on silica gel, which explains the low yields.

The inhibition and FP assays (Table 4) indicated that both **11a** and **11c** display a good affinity for *Mt* UGM and a strong inhibitory activity. These levels of affinity are comparable to the best heterocyclic UGM inhibitors reported to date that have been found in the low micromolar range (Fig. 5).^{10–13,15,23}

2.4. Antitubercular activity

The anti-tubercular activities of the best inhibitors of UGM (K_d < 70 μM) were then tested by determination of the minimal inhibitory concentration (MIC) against *M. tuberculosis* mc²6230 (Table 5). All compounds have MICs below or equal to 50 μg/mL, thus highlighting their potent anti-mycobacterial activity. Compounds **10a** and **10d** share MIC values comparable to the best UGM inhibitors reported so far (Entries 1 and 3).^{11,12,23}

3. Conclusion

This study revealed a new tricyclic structure with good affinity for *Mt* UGM and potent antitubercular activity and opens the door for subsequent SAR studies to generate derivatives with increased activity against drug susceptible and drug-resistant *Mt* strains.

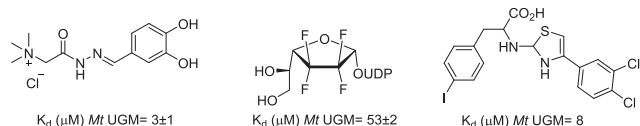
Fig. 5. Example of the best inhibitors of *Mt* UGM.^{10e,13,15}

Table 5

MIC values of *Mt* UGM inhibitors.

Entry	Compound	MIC ^[a] [μg/mL]
1	10a, R = H, R' = H	6.2
2	10c, R = OMe, R' = H	50
3	10d, R = [1,3]dioxolo, R' = H	3.1
4	11a, R = H, R' = CO ₂ H	50
5	11c, R = OMe, R' = CO ₂ H	50

^[a] The concentrations tested varied over a discrete 2-fold range: 1.5, 3.1, 6.2, 12.5, 25, 50, 100 μg/mL. MIC determinations were performed in duplicate on three independent occasions, with zero variation between experiments for the five compounds tested.

4. Experimental section

4.1. Chemistry

4.1.1. General methods

All reactions were carried out under argon atmosphere in dried glassware. Tetrahydrofuran was dried and freshly distilled from sodium and benzophenone. Dry DMF and catalysts were purchased from Sigma-Aldrich®. ¹H NMR spectra were recorded on a Bruker® Avance 300 (300 MHz) NMR spectrometer, using CDCl₃ as solvent. Data, reported using CHCl₃ (δ_H = 7.26 ppm) as internal reference, were as follows (in order): chemical shift (δ in ppm relative to CHCl₃), multiplicity (s, d, t, q, quint, m, br for singlet, doublet, triplet, quartet, quintuplet, multiplet, broad) and coupling constants (*J* in Hz). ¹³C NMR was recorded at 75 MHz on the same instrument, using the CDCl₃ solvent peak at (δ_C = 77.16 ppm) as reference. ¹⁹F NMR was recorded at 282 MHz on the same instrument. HRMS was obtained with a LCMS-IT-TOF mass spectrometer under conditions of ESI. IR spectra were recorded on a Perkin-Elmer Spectrum One spectrophotometer. Melting points were uncorrected.

4.1.2. Preparation of butenolides compounds.

A sealed tube was loaded with (*E*)-2,3-dibromobut-2-enoic acid (3 g, 12.3 mmol, 1 equiv.) and potassium carbonate (3.4 g, 24.6 mmol, 2 equiv.) in DMF (30 mL). The mixture is degassed with argon for 10 min. 3-Methylbut-1-yne (6 mL, 61.5 mmol, 5 equiv.) and copper iodide (2.3 g, 12.3 mmol, 1 equiv.) were added. The tube was filled with argon and sealed. The solution was stirred at 60 °C overnight, then hydrolyzed with aqueous saturated solution of NH₄Cl (100 mL) and filtered on Celite®. The filtrate was extracted with AcOEt (300 mL). The organic phase was washed with aqueous saturated solution of NH₄Cl (50 mL × 3), saturated solution of NaCl (50 mL), dried over anhydrous MgSO₄, filtered and solvents were evaporated under vacuum. The residue was purified by recrystallization in CH₂Cl₂ to afford the expected compound.

(Z)-3-Bromo-4-methyl-5-(2-methylpropylidene)furan-2(5H)-one (1): C₉H₁₁BrO₂, MW = 231.09 g/mol, yield = 74%, white solid, mp = 93–95 °C. IR (ATR) ν (cm⁻¹) = 2964, 2868, 1760, 1674, 1222, 995, 963, 870. ¹H NMR (300 MHz, CDCl₃) δ (ppm) = 5.27 (d, *J* = 9.7 Hz, 1H), 3.00 (dsept, *J* = 9.7 Hz, 6.8 Hz, 1H), 2.12 (s, 3H), 1.10 (d, *J* = 6.8 Hz, 6H). ¹³C NMR (75 MHz, CDCl₃) δ (ppm) = 165.2 (C=O), 151.3 (C), 147.6 (C), 121.2 (CH), 110.1 (C), 26.2 (CH), 22.6 (2CH₃), 11.7 (CH₃). HRMS (ESI) calcd. for C₉H₁₂⁸¹BrO₂ [M + H]⁺: 233.00002; found: 232.99946.

General procedure for Suzuki coupling, conditions A: In a Schlenk tube under argon, boronic acid (1.3 mmol, 1.2 equiv.), sodium

carbonate (1 M in H₂O, 1.3 mL, 1 mmol, 1.2 equiv.) and tetrakis(triphenylphosphine)palladium(0) (100 mg, 0.087 mmol, 10 mol%) were added to a solution of (Z)-3-bromo-4-methyl-5-(2-methylpropylidene)furan-2(5H)-one (**1**) (250 mg, 1.08 mmol, 1 equiv.) in toluene and ethanol (6:4, 10 mL/6 mL). The resulting mixture was stirred for 8 h at 80 °C, cooled at room temperature and filtered on Celite®. The solvents were removed from the filtrate under the vacuum and water (10 mL) was added to the resulting residue. The aqueous phase was extracted with diethyl ether (3 × 20 mL). The combined organic phases were washed with brine (25 mL), dried over anhydrous MgSO₄, filtered and solvents were evaporated under vacuum. The residue was purified by column chromatography on silica gel with petroleum ether/EtOAc as eluent to afford expected compound.

(Z)-3-(4-Fluorophenyl)-4-methyl-5-(2-methylpropylidene)furan-2(5H)-one (2a): C₁₅H₁₅FO₂, MW = 246.28 g/mol, yield = 67%, white solid, mp = 87–89 °C. IR (ATR) ν (cm⁻¹) = 2967, 2870, 1743, 1663, 1590, 1508, 1224, 979, 837. ¹H NMR (300 MHz, CDCl₃) δ (ppm) = 7.52 (dd, *J* = 8.8 Hz, 5.4 Hz, 2H), 7.14 (t, *J* = 8.8 Hz, 2H), 5.26 (d, *J* = 9.6 Hz, 1H), 3.08 (dsept, *J* = 9.6 Hz, 6.7 Hz, 1H), 2.22 (s, 3H), 1.13 (d, *J* = 6.7 Hz, 6H). ¹⁹F NMR (282 MHz, CDCl₃) δ (ppm) = -112.0. ¹³C NMR (75 MHz, CDCl₃) δ (ppm) = 169.2 (C=O), 162.8 (d, *J* = 248 Hz, C-F), 148.3 (C), 146.9 (C), 131.0 (d, *J* = 8 Hz, 2CH), 126.2 (d, *J* = 3 Hz, C), 125.6 (C), 120.2 (CH), 115.8 (d, *J* = 22 Hz, 2CH), 26.4 (CH), 22.8 (2CH₃), 11.1 (CH₃). HRMS (ESI) calcd. for C₁₅H₁₆FO₂ [M + H]⁺: 247.11288; found: 247.11222.

(Z)-3-([1,1'-Biphenyl]-4-yl)-4-methyl-5-(2-methylpropylidene)furan-2(5H)-one (2b): C₂₁H₂₀O₂, MW = 304.39 g/mol, yield = 66%, white paste. IR (ATR) ν (cm⁻¹) = 2963, 1760, 1598, 1583, 1572, 1479, 1452, 1383, 1265, 1172, 921, 805, 755, 735, 698. ¹H NMR (300 MHz, CDCl₃) δ (ppm) = 7.74–7.72 (m, 1H), 7.62–7.58 (m, 3H), 7.55–7.51 (m, 2H), 7.49–7.43 (m, 2H), 7.36 (m, 1H), 5.27 (d, *J* = 9.6 Hz, 1H), 3.11 (dsept, *J* = 9.6 Hz, 6.8 Hz, 1H), 2.27 (s, 3H), 1.14 (d, *J* = 6.7 Hz, 6H). ¹³C NMR (75 MHz, CDCl₃) δ (ppm) = 169.2 (C=O), 148.4 (C), 147.3 (C), 141.7 (C), 140.8 (C), 131.5 (C), 126.3 (C), 129.1 (CH), 129.0 (2CH), 128.0 (CH), 127.9 (CH), 127.7 (CH), 127.5 (CH), 127.4 (2CH), 120.1 (CH), 26.4 (CH), 22.9 (2CH₃), 11.2 (CH₃). HRMS (ESI) calcd. for C₂₁H₂₁O₂ [M + H]⁺: 305.15361; found: 305.15286.

(Z)-3-(6-Methoxynaphthalen-2-yl)-4-methyl-5-(2-methylpropylidene)furan-2(5H)-one (2c): C₂₀H₂₀O₃, MW = 308.38 g/mol, yield = 61%, white solid, mp = 144–146 °C. IR (ATR) ν (cm⁻¹) = 2964, 1749, 1664, 1628, 1595, 1483, 1217, 988, 880, 809. ¹H NMR (300 MHz, CDCl₃) δ (ppm) = 7.96 (d, *J* = 1.4 Hz, 1H), 7.79 (dd, *J* = 8.6 Hz, 3.5 Hz, 2H), 7.61 (dd, *J* = 8.7 Hz, 1.8 Hz, 1H), 7.19–7.13 (m, 2H), 5.26 (d, *J* = 9.6 Hz, 1H), 3.94 (s, 3H), 3.12 (dsept, *J* = 9.6 Hz, 6.8 Hz, 1H), 2.29 (s, 3H), 1.14 (d, *J* = 6.8 Hz, 6H). ¹³C NMR (75 MHz, CDCl₃) δ (ppm) = 169.5 (C=O), 158.5 (C), 148.5 (C), 146.5 (C), 134.4 (C), 130.1 (CH), 128.7 (C, CH), 127.1 (CH), 126.8 (CH), 126.6 (C), 125.4 (C), 119.6 (CH), 119.4 (CH), 105.7 (CH), 55.5 (CH₃), 26.4 (CH), 22.9 (2CH₃), 11.2 (CH₃). HRMS (ESI) calcd. for C₂₀H₂₁O₃ [M + H]⁺: 309.14907; found: 309.14832.

(Z)-4-Methyl-5-(2-methylpropylidene)-3-(pyridin-4-yl)furan-2(5H)-one (2d): C₁₄H₁₅NO₂, MW = 229.28 g/mol, yield = 84%, yellow oil. IR (ATR) ν (cm⁻¹) = 3054, 2961, 2869, 1754, 1664, 1577, 1437, 1297, 1192, 1119, 1032, 972, 878, 694. ¹H NMR (300 MHz, CDCl₃) δ (ppm) = 8.74 (d, *J* = 1.5 Hz, 1H), 8.62 (dd, *J* = 4.9 Hz, 1.4 Hz, 1H), 8.03 (dt, *J* = 8.0 Hz, 1.9 Hz, 1H), 7.45 (ddd, *J* = 8.0 Hz, 4.9 Hz, 0.6 Hz, 1H), 5.35 (d, *J* = 9.6 Hz, 1H), 3.09 (dsept, *J* = 9.6 Hz, 6.8 Hz, 1H), 2.29 (s, 3H), 1.14 (d, *J* = 6.7 Hz, 6H). ¹³C NMR (75 MHz, CDCl₃) δ (ppm) = 168.7 (C), 149.5 (CH), 149.4 (CH), 148.4 (C), 148.2 (C), 136.6 (CH), 126.5 (C), 123.6 (CH), 123.5 (C), 121.3 (CH), 26.5 (CH), 22.7 (2CH₃), 11.2 (CH₃). HRMS (ESI) calcd. for C₁₄H₁₆NO₂ [M + H]⁺: 230.11756; found: 230.11699.

(Z)-4-Methyl-5-(2-methylpropylidene)-[3,3'-bifuran]-2(5H)-one (2e): C₁₃H₁₄O₃, MW = 218.25 g/mol, yield = 64%, white solid,

mp = 64–66 °C. IR (ATR) ν (cm⁻¹) = 3155, 3134, 2958, 2870, 1756, 1669, 1545, 1467, 1304, 1205, 1157, 1021, 964, 931, 830, 800, 740, 644, 601. ¹H NMR (300 MHz, CDCl₃) δ (ppm) = 8.07 (bs, 1H), 7.50 (t, *J* = 1.8 Hz, 1H), 6.82 (dd, *J* = 1.8 Hz, 0.8 Hz, 1H), 5.21 (d, *J* = 9.6 Hz, 1H), 3.06 (dsept, *J* = 9.6 Hz, 6.7 Hz, 1H), 2.24 (s, 3H), 1.11 (d, *J* = 6.7 Hz, 6H). ¹³C NMR (75 MHz, CDCl₃) δ (ppm) = 168.8 (C), 148.6 (C), 143.8 (C), 143.4 (CH), 142.9 (CH), 119.4 (CH), 119.1 (C), 115.8 (C), 108.9 (CH), 26.4 (CH), 22.9 (2CH₃), 11.1 (CH₃). HRMS (ESI) calcd. for C₁₃H₁₅O₃ [M + H]⁺: 219.10212; found: 219.10100.

(Z)-3-(Benzofuran-2-yl)-4-methyl-5-(2-methylpropylidene)

furan-2(5H)-one (2f): C₁₇H₁₆O₃, MW = 268.31 g/mol, yield = 62%, white solid, mp = 87–89 °C. IR (ATR) ν (cm⁻¹) = 2961, 2928, 2865, 1750, 1669, 1443, 1297, 1216, 1123, 1037, 995, 925, 824, 751, 659. ¹H NMR (300 MHz, CDCl₃) δ (ppm) = 7.63 (dd, *J* = 7.4 Hz, 1.0 Hz, 1H), 7.56 (s, 1H), 7.50 (dd, *J* = 7.4 Hz, 0.8 Hz, 1H), 7.33 (td, *J* = 7.3 Hz, 1.4 Hz, 1H), 7.25 (td, *J* = 7.4 Hz, 1.2 Hz, 1H), 5.36 (d, *J* = 9.7 Hz, 1H), 3.09 (dsept, *J* = 9.6 Hz, 6.7 Hz, 1H), 2.55 (s, 3H), 1.14 (d, *J* = 6.7 Hz, 6H). ¹³C NMR (75 MHz, CDCl₃) δ (ppm) = 167.3 (C=O), 155.0 (C), 148.7 (C), 148.6 (C), 145.2 (C), 128.2 (C), 125.5 (CH), 123.4 (CH), 122.0 (CH), 121.3 (CH), 116.7 (C), 111.2 (CH), 108.4 (CH), 26.6 (CH), 22.8 (2CH₃), 11.4 (CH₃). HRMS (ESI) calcd. for C₁₇H₁₇O₃ [M + H]⁺: 269.11722; found: 269.11698.

4.1.3. Preparation of new oxazinoindoles **11a** and **11c**

Aryl iodide (260 mg, 0.6 mmol), alkyne (0.9 mmol), triphenylphosphine (15 mg, 10% mol), CuI (11 mg, 10% mol), and triethylamine (120 μ L, 0.9 mmol) were combined with DMF (4.0 mL) in schlenk sealing tube. The resulting reaction mixture was stirred under argon for overnight at room temperature or for 2 h on MW at 50 °C. The solvent was removed from the reaction mixture under the vacuum and the resulting crude product was purified by flash chromatography on silica gel (petroleum ether/AcOEt = 100:0 to 50:50).

(E)-7-(10-Iodo-8-methoxy-1-oxo-1H-[1,4]oxazino[4,3-a]indol-3(4H)-ylidene)hept-5-ynoic acid (11a): C₁₉H₁₆INO₅, MW = 465.24 g/mol, yield = 12%, yellow solid, mp = 177–179 °C. IR (ATR) ν (cm⁻¹) = 3050, 2891, 1744, 1696, 1645, 1508, 1412, 1378, 1308, 1227, 1194, 1076, 922, 737. ¹H NMR (300 MHz, CDCl₃) δ (ppm) = 7.62 (d, *J* = 8.2 Hz, 1H), 7.50 (dd, *J* = 6.8 Hz, 1.0 Hz, 1H), 7.42 (d, *J* = 8.4 Hz, 1H), 7.31 (dd, *J* = 6.8 Hz, 1.0 Hz, 1H), 5.65 (m, 1H), 5.15 (d, *J* = 0.8 Hz, 2H), 2.59–2.51 (m, 4H), 1.95 (quint, *J* = 6.9 Hz, 2H). ¹³C NMR (75 MHz, CDCl₃) δ (ppm) = 177.4 (C), 154.3 (C), 151.4 (C), 136.9 (C), 131.3 (C), 130.0 (CH), 124.3 (CH), 122.9 (CH), 121.0 (C), 110.6 (CH), 97.1 (C), 96.0 (CH), 74.3 (C), 69.4 (C), 40.8 (CH₂), 32.7 (CH₂), 23.6 (CH₂), 19.2 (CH₂). HRMS (ESI) calcd. For C₁₈H₁₅INO₄ [M + H]⁺: 436.0046, found 436.0034.

(E)-7-(10-Iodo-1-oxo-1H-[1,4]oxazino[4,3-a]indol-3(4H)-ylidene)hept-5-ynoic acid (11c): C₁₈H₁₄INO₄, MW = 435.00 g/mol, yield = 14%, yellow solid, mp = 157–159 °C. IR (ATR) ν (cm⁻¹) = 3066, 2929, 1741, 1705, 1638, 1510, 1433, 1313, 1281, 1236, 1195, 1080, 953, 917, 834, 809, 739. ¹H NMR (300 MHz, CDCl₃) δ (ppm) = 7.30 (d, *J* = 9.1 Hz, 1H), 7.12 (dd, *J* = 9.1 Hz, 2.4 Hz, 1H), 6.89 (d, *J* = 2.3 Hz, 1H), 5.67–5.64 (m, 1H), 5.11 (d, *J* = 1.0 Hz, 2H), 3.90 (s, 3H), 2.59–2.51 (m, 4H), 1.95 (quint, *J* = 7.0 Hz, 2H). ¹³C NMR (75 MHz, CDCl₃) δ (ppm) = 177.3 (C), 156.4 (C), 154.2 (C), 151.5 (C), 132.2 (C), 131.8 (C), 120.9 (CH), 120.4 (CH), 111.7 (CH), 103.2 (CH), 97.0 (C), 95.8 (CH), 74.4 (C), 68.2 (C), 55.9 (CH₃), 40.9 (CH₂), 32.6 (CH₂), 23.6 (CH₂), 19.2 (CH₂). HRMS (ESI) calcd. For C₁₈H₁₅INO₄ [M + H]⁺: 436.00403, found: 436.0034.

4.2. Docking

Molecular docking studies were carried out using GOLD v 5.3.²⁴ GOLD is based on a genetic algorithm and allows to perform docking of flexible ligands inside proteins with partial flexibility in the

neighborhood of the active site. The crystal structure used as macro-molecular receptor was *Mt* UGM in closed form with the substrate bound (PDB code: 4RPG). Prior to docking calculation, water molecules and the bound substrate UDP-Galp were removed from the crystal structure. The inhibitors docked conformations were obtained using the score function ChemPLP.²⁵ Examination of the structures of the complex were carried out using PyMOL software.

4.3. *Mt* UGM inhibitory activity

UGM preparation: A vector construct (pET-29b) containing the gene encoding for UGM from *Mt* was provided by Prof. Laura L. Kiessling. The overexpression and UGM purification followed our previously published procedure.¹²

HPLC assay: Inhibition of UGM was performed following the procedure already described by Liu et al.²⁶ as well as by our group.²⁷ All assays were performed at room temperature using a phosphate buffer (NaH₂PO₄ 100 mM, pH 7.4), and fresh solutions of sodium dithionite which provide reductive conditions. The activity of the enzyme (in the presence and in the absence of an inhibitor) is evaluated by measuring the conversion of UDP- α -Galp into UDP- α -Galp. The enzyme (60 nM *Mt* UGM) in phosphate buffer was first pre-incubated for 5 min, then reduced with sodium dithionite (final concentration 12.5 mM) and incubated for specific time at room temperature, in absence and presence of inhibitor. The substrate UDP- α -Galp (final concentration 25 μ M) was added and allowed the reaction to proceed at five different times. The reaction was stopped by quenching the samples with liquid N₂. The conversion of UDP- α -Galp into UDP- α -Galp was monitored by HPLC (Waters 600 E with a C₁₈ Atlantis T3 column, 5 μ M 4.6 \times 250 mm, elution with 50 mM triethylamine acetic acid pH 6.8, 0.5% CH₃CN; UV detection at 262 nm and flow rate 1 mL/min).

FP assay. The assay described by Kiessling et al. was strictly followed, including the synthesis of the fluorescent probe (UDP-fluorescein).¹⁶ To determine the binding affinity of UDP-fluorescein towards *Mt* UGM, serial dilutions of dialyzed UGM (final concentration: 1×10^{-5} to 10 μ M) were incubated with 18 nM of the fluorescent probe in 50 mM sodium phosphate buffer, pH 7.0 at room temperature. Final volumes were 30 μ L in 384 well black microtiter plates and the measurements were realized in triplicate. Fluorescence polarization was analyzed using DTX880 Multimode Detector Beckman-Coulter device ($\lambda_{\text{excitation}} = 485$ nm, $\lambda_{\text{emission}} = 535$ nm).

4.4. *In vitro* anti-tubercular activity

Antitubercular evaluations were performed against the avirulent, pantothenate-auxotrophic *Mt* mc²6230 strain²⁸ cultured in 7H9 (Middlebrook) broth supplemented with oleic-albumin-dextrose-catalase enrichment (OADC) and 109 μ M pantothenic acid (complete 7H9 medium) at 37 °C without agitation. MIC determination was done using the broth dilution method. Briefly, a log-phase (OD₆₀₀ ~ 1) culture was diluted to an OD₆₀₀ = 0.05 in complete 7H9 medium and deposited in all the wells of a 96 well microtiter plate (for the first row 200 μ L/well, for all other rows 100 μ L/well). The tested compounds were then directly added (2 μ L per well of a 10 mg/mL stock solution) to the first row wells. Serial 2-fold dilutions were then done starting from the first row. As a measure to minimize evaporation of media, plates were wrapped in plastic. They were then placed in a 37 °C incubator and observed after 7 days. Control wells included a control for the vehicle that compounds were dissolved in (DMSO), in which bacterial growth was not inhibited (as for untreated wells) and wells containing a drug with known anti-tubercular activity (INH), in which bacterial growth was inhibited at ~30 ng/mL in line with the reported MIC of this drug.²⁹ The MIC was

defined as the lowest concentration of compound at which no visible bacterial growth (change in turbidity) was observed.

Declaration of Competing Interest

The authors declare that they have no known competing financial interests or personal relationships that could have appeared to influence the work reported in this paper.

Acknowledgments

This study was supported by the Fondation pour la Recherche Médicale (grant DEQ20150331719 to L.K.), the Association Gregory Lemarchal and Vaincre la Mucoviscidose (grant RIF20180502320 to C.R.) The University of Namur (PhD grant to SV) and China Scholarship Council (PhD grant to JF). We acknowledge the French Ministry for Research and Innovation for the financial support and Dr. Frédéric Montigny (Analysis Department, Tours University) for HRMS.

Appendix A. Supplementary data

Supplementary data to this article can be found online at <https://doi.org/10.1016/j.bmc.2020.115579>.

References

1. “Antibacterial agents in clinical development. An analysis of the antibacterial clinical development pipeline, including tuberculosis”, September 2017, World Health Organization.
2. Koul A, Arnould E, Lounis N, Guillemont J, Andries K. *Nature*. 2011;469:483–490.
3. Brennan PJ. *Tuberculosis (Edinb)*. 2003;83:91–97.
4. (a) Karakousis PC, Bishai WR, Dorman SE. *Cell Microbiol*. 2004;6:105–116
(b) Ruhl CR, Pasko BL, Khan HS, et al. *Cell*. 2020;181:1–13.
5. (a) Guerardel Y, Maes E, Ellass E, et al. *J Biol Chem*. 2002;277:30635–30648
(b) Vignat C, Guérardel Y, Kremer L, et al. *J Immunol*. 2003;171:2014–2023
(c) Briken V, Porcelli SA, Besra GS, Kremer L. *Mol Microbiol*. 2004;53:391–403
(d) Birch HL, Alderwick LJ, Appelmek BJ, et al. *Proc Natl Acad Sci USA*. 2010;107:2634–2639.
6. (a) Brennan PJ, Crick DC. *Curr Top Med Chem*. 2007;7:475–488
(b) Nzila A, Ma Z, Chibale K. *Future Med Chem*. 2011;3:1413–1426.
7. (a) Makarov V, Manina G, Mikusova K, et al. *Science*. 2009;324:801–804
(b) Christophe T, Jackson M, Jeon HK, et al. *PLoS Pathog*. 2009;5:e1000645.
8. (a) Kremer L, Dover LG, Morehouse C, et al. *J Biol Chem*. 2001;276:26430–26440
(b) Richards MR, Lowary TL. *ChemBioChem*. 2009;10:1920–1938
(c) Eppe G, El Bkassiny S, Vincent SP. Galactofuranose biosynthesis: discovery, mechanisms and therapeutic relevance. In: Jimenes-Barbeo J, Cañada FJ, Martin-Santamaria S, eds. *Carbohydrates in Drug Design and Discovery*. RSC; 2015:209–241.
9. (a) Sanders DAR, Staines AG, McMahon SA, McNeil MR, Whitfield C, Naismith JH. *Nat Struct Biol*. 2001;8:858–863
(b) Konyariková Z, Savková K, Kozmo S, Mikušová K. *Antibiotics*. 2020;9:20.
10. (a) van Straaten KE, Kuttivatveetil JRA, Sevrain CM, et al. *J Am Chem Soc*. 2015;137:1230–1244
(b) Errey JC, Mann MC, Fairhurst SA, et al. *Org Biomol Chem*. 2009;7:1009–1016
(c) Yuan Y, Bleile DW, Wen X, et al. *J Am Chem Soc*. 2008;130:3157–3168
(d) El Bkassiny S, N’Go I, Sevrain CM, Tikad A, Vincent SP. *Org Lett*. 2014;16:2462–2465
(e) N’Go I, Golten S, Ana Ardá J, et al. *Chem Eur J*. 2014;20:106–112
(f) Dumitrescu L, Eppe G, Tikad A, et al. *Chem Eur J*. 2014;20:15208–15215
(g) Caravano A, Vincent SP. *Eur J Org Chem*. 2009:1771–1780
(h) Dhatwalia R, Singh H, Solano LM, et al. *J Am Chem Soc*. 2012;134:18132–18138.
11. Kincaid VA, London N, Wangkanont K, et al. *ACS Chem Biol*. 2015;10:2209–2218 and cited references.
12. Villaume SA, Fu J, N’Go I, et al. *Chem Eur J*. 2017;10423–10429.
13. Fu J, Fu H, Dieu M, et al. *Chem Commun*. 2017;53:10632–10635.
14. Kiessling LL, Winton VJ, Justen AM. *US Pat Appl Publ*. 2017 US 20170258805 A1 20170914.
15. Dykhuizen EC, May JF, Tongpenyai A, Kiessling LL. *J Am Chem Soc*. 2008;130:6706–6707.
16. Carlson EE, May JF, Kiessling LL. *Chem Biol*. 2006;13:825–837.
17. Kuhnt D, Anke T, Besl H, et al. *J Antibiot*. 1990;43:1413–1420.
18. (a) Miao S, Andersen RJ. *J Org Chem*. 1991;56:6275–6280
(b) Kotora M, Negishi E. *Synthesis*. 1997:121–128

- (c) Gallo GG, Coronelli C, Vigevani A, Lancini GC. *Tetrahedron*. 1969;25:5677–5680.
19. (a) Liu F, Negishi E. *J Org Chem*. 1997;62:8591–8594
(b) Von der Ohe F, Brückner R. *Tetrahedron Lett*. 1998;39:1909–1910.
20. Inack-Ngi S, Rahmani R, Commeiras L, et al. *Adv Synth Catal*. 2009;351:779–788.
21. Thanikachalam PV, Maurya RK, Garg V, Monga V. *Eur J Med Chem*. 2019;180:562–612.
22. Hammoud S, Anselmi E, Cherry K, Kizirian J-C, Thibonnet J. *Eur J Org Chem*. 2018:6314–6327.
23. Winton VJ, Aldrich C, Kiessling LL. *ACS Infect Dis*. 2016;2:538–543.
24. Verdonk ML, Cole JC, Hartshorn MJ, Murray CW, Taylor RD. *Prot Struct Func Bioinform*. 2003;52:609–623.
25. Liebeschuetz J, Cole J, Korb O. *J Comput Aided Mol Des*. 2012;26:737–748.
26. Itoh K, Huang Z, Liu H-W. *Org Lett*. 2007;9:879–882.
27. (a) Eppe G, Peltier P, Daniellou R, Nugier-Chauvin C, Ferrières V, Vincent SP. *Bioorg Med Chem Lett*. 2009;19:814–816
(b) Ansiaux C, N'Go I, Vincent SP. *Chem Eur J*. 2012;18:14860–14866.
28. Sambandamurthy VK, Derrick SC, Tsungda Hsu B, et al. *Vaccine*. 2006;24:6309–6320.
29. Kremer L, Douglas JD, Baulard AR, et al. *J Biol Chem*. 2000;275:16857–16864.